

Clouds and Chemistry: Brown Dwarf Atmospheric Properties from Optical and Infrared Colors

M. S. Marley² S. Seager³ D. Saumon⁴ K. Lodders⁵ A. S. Ackerman¹, R. Freedman¹

ABSTRACT

The optical and infrared colors of L and T dwarfs are sensitive to cloud sedimentation and chemical processes in their atmospheres. In particular the $J - K$ color of a cooling brown dwarf is sensitive to the vertical distribution of condensates in its atmosphere. Only atmosphere models which include sedimentation of condensates are able to reproduce the observed trends in $J - K$ in which objects first become redder, then bluer with falling effective temperature. The Sloan Digital Sky Survey color $i' - z'$ is sensitive to assumptions surrounding the alkali metal chemistry. Chemical equilibrium models which account for cloud sedimentation predict redder colors, by up to 2 magnitudes, than models which neglect sedimentation. The $i' - z'$ vs. $J - K$ color-color diagram is thus interesting for the window it opens into diverse atmospheric processes. In addition, we predict the locus in this color-color diagram of brown dwarfs cooler than yet found.

1. Introduction

The Sloan Digital Sky Survey (SDSS) and the 2-Micron All Sky Survey (2MASS) have both had great success in discovering L and T type brown dwarfs. In the SDSS system, all brown dwarfs are easily identified as they are uniquely red in $i' - z'$. In the 2MASS color system, the identification of brown dwarfs is somewhat muddled since L dwarfs are red in 2MASS $J - K_s$ color ($1 \leq J - K_s \leq 2$) while the cooler T dwarfs like Gliese 229 B are bluer ($J - K_s < 0.5$) (Kirkpatrick et al. 1999; Burgasser et al. 1999; Burgasser et al. 2000). As a consequence, it is difficult to distinguish early-T type brown dwarfs ($J - K_s \sim 1$; formerly called L/T transition dwarfs) from M-dwarfs with similar colors from 2MASS data alone. While the mechanisms responsible for the $J - K_s$ and the $i' - z'$ colors of the L and T dwarfs are understood, there has yet been no single theory that self-consistently describes the evolution of brown dwarfs in this color space.

¹NASA Ames Research Center, MS 245-5, Moffett Field CA, 94035

²New Mexico State University; Department of Astronomy; Las Cruces NM 88003

³Institute for Advanced Study, Einstein Drive, Princeton, NJ 08540

⁴Department of Physics and Astronomy, Vanderbilt University, Nashville, TN 37235

⁵Planetary Chemistry Laboratory, Department of Earth and Planetary Sciences, Washington University, St. Louis, MO 63130-4899

Because of their intrinsic faintness, moderate to high resolution spectroscopy may not be performed on all of the 300 or so known and expected brown dwarfs discovered by these surveys. Thus analyses of brown dwarf colors could be essential to provide information on the brown dwarf physical properties. We have explored the utility of a number of i' , z' , J , H , and K color-color diagrams for constraining brown dwarf physical properties and find the $i' - z'$ vs. $J - K$ diagram particularly interesting. First these are essentially the colors in which SDSS and 2MASS discover brown dwarfs⁶. Second, alkali metals dominate the $i' - z'$ colors while H_2O and CH_4 absorption bands and cloud physics control the $J - K$ colors. Over the pressure and temperature ranges of interest, the chemical pathways of alkali and $H_2O/CH_4/CO$ are weakly coupled, thus this particular color-color diagram reflects a remarkably diverse set of influences.

In this Letter, we describe how clouds and the chemistry of carbon, oxygen and alkali elements (mainly potassium) control the 2MASS and SDSS colors used to discover brown dwarfs and we explore the potential of the $i' - z'$ vs. $J - K$ color-color diagram as a tool to deduce the physical characteristics of brown dwarfs and the physics of their atmospheres. We also predict the colors of very cool brown dwarfs ($T_{\text{eff}} \lesssim 700$ K) yet to be discovered.

2. Color Trends

Brown dwarfs are notoriously different from blackbodies of the same effective temperature. Figure 1 shows the $i' - z'$ vs. $J - K$ colors for observed SDSS L (triangles) and T (squares) dwarfs (Strauss et al. 1999; Fan et al. 2000; Leggett et al. 2000; Tsvetanov et al. 2000). The brown dwarfs are spread out over several magnitudes in both $i' - z'$ and $J - K$. In addition, they are located in very different parts of this diagram.

Blackbodies get redder in all colors with decreasing T_{eff} as the Planck peak shifts redward; a temperature sequence of blackbody emitters in Figure 1 would follow a diagonal line cutting from blue to red through the extreme upper left corner of the color-color diagram. Brown dwarfs, however, are subject to a more complex set of influences and first become redder and then bluer in $J - K$ as they age and cool. The initial reddening arises as progressively more condensate is found in the visible atmospheres in the range from $T_{\text{eff}} \sim 2000$ to ~ 1400 K. Then $J - K$ turns blueward because in the cooler brown dwarfs the cloud base (and thus most of the cloud opacity) falls below the photosphere (Marley 2000; Ackerman & Marley 2001; Tsuji 2001; Allard et al. 2001), leaving the visible atmosphere relatively clear of condensates. In the absence of clouds, water, pressure-induced absorption by molecular hydrogen, and mostly methane act to rapidly close the K band infrared window as T_{eff} falls, resulting in increasingly blue $J - K$.

In the optical, brown dwarfs become redder with decreasing T_{eff} . This trend is produced by the growing importance of the $0.59\mu\text{m}$ Na I and $0.77\mu\text{m}$ K I resonance doublets (Tsuji, Ohnaka

⁶Note that 2MASS employs the K_s filter in its survey.

& Aoki 1999; Burrows, Marley, & Sharp 2000) with falling T_{eff} ; as the brown dwarf cools, the gradual disappearance of TiO and cloud opacity with decreasing T_{eff} leaves a progressively more transparent atmosphere at optical wavelengths. The K I resonance doublet is centered on the i' band while the z' band is only affected by the far red wing, producing very red $i' - z'$ colors (Fig. 2).

Brown dwarfs with T_{eff} and infrared colors intermediate between the coolest and reddest L dwarfs and the much cooler and bluer T dwarfs like Gl 229 B were initially thought to be rare since 2MASS found few of them (Kirkpatrick et al. 2000). T dwarfs with $1100 \lesssim T_{\text{eff}} \lesssim 1300$ K are difficult to discover in the 2MASS $J - K_s$ color because they are mixed with the far more numerous and hotter M dwarfs. The SDSS optical colors do not suffer from this infrared color degeneracy in this T_{eff} range. The SDSS collaboration has published the discovery of three brown dwarfs with $J - K$ colors lying between 0.5 and 1 (formerly called L/T transition objects; see Leggett et al. 2000) and has now typed them as early T dwarfs (Geballe et al. in preparation). The SDSS project is expected to find many more brown dwarfs in the near future.

3. Model Atmospheres

To model the colors of solar metallicity L and T dwarfs we employ the radiative-convective equilibrium atmosphere model of Marley et al. (1996; further described in Burrows et al. 1997). The model has been updated to include alkali opacities as described in Burrows et al. (2000) and the precipitating cloud model of Ackerman & Marley (2001). High resolution spectra are computed from these atmosphere models (temperature profile and cloud structure) with a spectral synthesis code (Saumon et al. 2000; Geballe et al. 2001). In the high-resolution spectra, the non-isotropic scattering by dust particles is mapped onto an equivalent isotropic scattering problem following the prescription given in Chamberlain & Hunten (1987). Theoretical colors in turn are calculated from the high resolution synthetic spectra. For J and K colors we use the Mauna Kea Observatory Near Infrared System⁷ and for SDSS the i' and z' filter functions and the SDSS definition of magnitude (Fukugita et al. 1996).

The calculation of chemical equilibrium in an atmosphere is dependent upon the assumptions made regarding the fate of condensates. In a gravitational field, atmospheric constituents that condense tend to fall. If the condensate is liquid water meteorologists term it rain. We consider two different chemical equilibrium models. In the first case there is no sedimentation of condensates. For this we use the baseline model from Burrows and Sharp (1999; hereafter BS99). In the second case we treat sedimentation with the cloud condensation model developed by Lewis (1969) for Jovian planets and used by Fegley and Lodders (1996), Lodders (1999), and Lodders and Fegley (2001) for brown dwarfs.

For the radiative transfer calculations the clouds are assumed to be homogeneous horizontally

⁷<http://www.ifa.hawaii.edu/~tokunaga/filterSpecs.html>

and are modeled following the approach developed by Ackerman & Marley (2001). In this model the upward eddy transport of condensable gas and condensate is balanced by efficient downward loss by precipitation. The efficiency of sedimentation is parameterized by f_{rain} with larger values denoting greater sedimentation efficiency and optically thinner clouds. Ackerman & Marley (2001) find that $f_{\text{rain}} = 3$ best models the observed ammonia cloud deck on Jupiter. Note that there is a slight inconsistency between the vertical distribution of condensates in the chemical equilibrium model (using the vertical profile described by Lewis (1969)) and the radiative transfer cloud model (using the model of Ackerman & Marley (2001)). However, the vertical condensate profiles with moderate values of f_{rain} are similar to those predicted by the Lewis model. See Ackerman & Marley (2001) for more details.

For the purposes of comparison, we have also computed a sequence of cloudless models. In these models, the formation of condensates is taken into account in the calculation of the chemical equilibrium but the opacity of condensates is ignored in the calculation of radiative transfer. This is similar to the COND model of Allard et al. (2001).

4. The optical-IR Color-Color Diagram

Figure 1 shows a temperature sequence of brown dwarfs models in the $i' - z'$ vs. $J - K$ color-color diagram. Models are plotted for a fixed surface gravity of 1000 m s^{-2} , corresponding roughly to a mass of 35 Jupiter masses (M_J). Note that the surface gravity, g , of a given object increases as it contracts and cools, so for a given brown dwarf the cooling track will follow a slightly different path. Paths for brown dwarfs of different masses, however, are almost degenerate in the color-color diagram because the temperature at which optical depth $2/3$ is reached as a function of wavelength depends only weakly on the gravity. All surface gravities very nearly overlap in the $i' - z'$ vs. $J - K$ color-color diagram. So although T_{eff} may be estimated, there is no unique (T_{eff}, g) solution for given $i' - z'$ and $J - K$ colors.

The $i' - z'$ vs. $J - K$ color-color diagram is very sensitive to T_{eff} because of the disparate chemistry governing the two colors. The alkali metal chemistry for the observed brown dwarfs shown in Figure 1 mostly consists of neutral K being depleted into molecules and solids. This process (see Lodders 1999 for a complete discussion) is not strongly coupled to the C/H/O chemistry that controls CO, CH₄ and H₂O formation. At even lower temperatures, K disappears into chloride and hydroxide gasses but the alkali chemistry is still only weakly coupled to the C, H, and O chemistry. Thus brown dwarfs at different T_{eff} are well separated in this color-color diagram. There is no degeneracy for different T_{eff} as found in most other color-color combinations (e.g. $H - K_s$ vs. $J - H$, $J - K_s$ vs. $I - J$ (see Kirkpatrick et al. 2000 and Tsuji 2001)).

4.1. Clouds

The behavior of the cloud layer as a function of T_{eff} is of primary astrophysical interest. Qualitatively, the base of the cloud occurs where the (T, P) structure of the atmosphere crosses the condensation curve of the main condensibles (silicate and iron at high temperatures, and water at lower temperatures). A cloud deck forms with a vertical profile determined by the cloud model (f_{rain} for the Ackerman & Marley model). Because in the region of interest the condensation temperature of relevant substances is a weak function of pressure, the base of the cloud layer occurs at a slowly increasing temperature, as T_{eff} decreases. On the other hand, the temperature of the photosphere is approximately T_{eff} . It follows that as T_{eff} decreases, the cloud layer gradually disappears below the observable level of the atmosphere. This phenomenon has been discussed by several authors (Chabrier et al. 2000; Marley 2000; Allard et al. 2001; Tsuji 2001).

The opacity of the gas in brown dwarfs is dominated by molecular bands and varies strongly with wavelength, in contrast to the nearly grey cloud opacity. Thus the above discussion is somewhat simplistic since the concept of photosphere is not well defined in brown dwarfs. While continuum opacities ensure that the photosphere corresponds approximately to a fixed physical level in normal stars, in brown dwarfs the visible and near-infrared spectrum can probe a range of depths of up to 6 pressure scale heights (Saumon et al. 2000)! This provides an opportunity to observationally probe the vertical structure of brown dwarf atmospheres and of the cloud layer in particular.

This sinking of the cloud layer below the “photosphere” as T_{eff} decreases is illustrated Figure 2 where the curves show the level in the atmosphere where the optical depth $\tau_{\nu} = 2/3$. Here, vertical position in the atmosphere is indicated by the local temperature. Three models are shown with $T_{\text{eff}} = 500, 1000, \text{ and } 1500 \text{ K}$ from top to bottom, respectively. A pair of curves is shown for each model; one showing the photosphere determined by gas opacity *only* and one for the nearly grey cloud opacity *only*. For the upper pair of curves ($T_{\text{eff}} = 500 \text{ K}$), the deep silicate and iron cloud photosphere lies below (at higher temperature) the gas photosphere at all wavelengths, implying that the cloud layer remains essentially invisible, and has little effect on the emergent spectrum. In the lower pair of curves ($T_{\text{eff}} = 1500 \text{ K}$), the cloud becomes opaque well above the gas photosphere in the $J, H, \text{ and } K$ bands. The cloud top is therefore observable in these three bandpasses (but not at other wavelengths) and the spectral energy distribution is strongly affected by the presence of the cloud.

Figure 2 clearly shows that the cloud layer disappears below the observable atmosphere over a range of T_{eff} , depending on the bandpass of observation. For example, the cloud becomes invisible in the K band for $T_{\text{eff}} \lesssim 1400 \text{ K}$ but remains detectable in the J band down to $T_{\text{eff}} \sim 800 \text{ K}$. The Ackerman & Marley cloud model with $f_{\text{rain}} = 5$ predicts that the spectra of all known T dwarfs are affected by clouds.

Observationally, one of the most interesting features in the $i' - z'$ vs. $J - K$ color-color diagram shown in Figure 1 is the reddening in $J - K$ of the L dwarfs which is not present in the T dwarfs. This difference in $J - K$ trajectory results from the presence of condensates in the photosphere

of the L dwarfs but not in the late T dwarfs. The blackbody-like condensate emission pushes L dwarfs to the red in $J - K$, despite the tug of water opacity towards the blue. This effect of condensate opacity is best illustrated by comparing the cloudless models (solid line) and the cloudy models ($f_{\text{rain}} = 5$, dotted line; $f_{\text{rain}} = 3$, dashed line;) in Figure 1a. The cloudless L dwarf models show a continuous blueward trend in $J - K$ with decreasing T_{eff} — because of increasing H_2O and pressure-induced H_2 absorption — in contradiction with the redward trend of the L dwarf data. The cloudy models on the other hand, match the redward trend in $J - K$ of the L dwarf data very well.

The progressively redder trend in L dwarf $J - K$ colors has been noted before (e.g. Kirkpatrick et al. 1999; Martin et al. 1999; Fan et al. 2000; Tsuji 2001) and demonstrated by spectral fitting to be caused by the appearance of more and more silicate condensates in the cooling brown dwarf atmospheres (e.g Leggett, Allard, & Hauschildt 1998; Chabrier et al. 2000; Marley 2000). However models in which there is no settling of the condensates (Chabrier et al. 2000) produce colors, particularly for the later L dwarfs, that are much too red. For example the dusty model of Chabrier et al. predicts that a 1 Gyr old 50 M_\odot brown dwarf with $T_{\text{eff}} = 1424\text{ K}$ will have $J - K = 3.9$ while our model with $f_{\text{rain}} = 5$ predicts $J - K \sim 1.2$. The muted $J - K$ colors of the reddest L dwarfs provide strong evidence of condensate sedimentation.

A second interesting feature in the $i' - z'$ vs. $J - K$ color-color diagram is the transition between the L and early T dwarfs that begins as a blueward turnover in $J - K$. The shape of the transition is not obvious from the color data, however (Figure 1). As the condensates sink below the visible atmosphere, the blackbody effect of the condensates is removed, halting the redward $J - K$ progression. The turnover occurs when the cloud layer is no longer visible in the K band (see Fig. 2). An important question has been the temperature range over which the L to T transition falls (e.g. Reid et al. 2001). The model T_{eff} at which the turnover begins as well as the maximum value of $J - K$ depend on the sedimentation parameter f_{rain} . For $f_{\text{rain}} = 5$, $J - K$ peaks at 1.5 ($T_{\text{eff}} = 1400\text{ K}$). Smaller values of f_{rain} produce thicker, more massive clouds whose tops remain in view in the J and K bands down to cooler T_{eff} . We find from Figure 1 that $f_{\text{rain}} \approx 5$ gives the best match of the observed turnover in $J - K$. This $J - K$ blueward turnover will be well characterized by future SDSS discoveries and the data will be essential for understanding cloud properties in brown dwarfs.

At some lower T_{eff} ($\sim 800\text{ K}$ for $f_{\text{rain}} = 5$) the temperature range where the condensate cloud base exists is below the visible photosphere. However the tops of the silicate clouds might still be limiting the depths from which flux emerges in the water and methane windows, thus accounting for the difficulty all cloudless models have had in correctly reproducing the ratio of the flux emerging from within and without of the water bands (Allard et al. 1996; Marley et al. 1996; Tsuji et al. 1996; Saumon et al. 2000; Geballe et al. 2001).

4.2. Alkali Metal Chemistry

The i' and z' band fluxes are diagnostic of alkali metal chemistry, mainly because they measure the core and the wing of the K I resonance doublet, respectively. In T dwarfs, the red wing of the doublet is detected up to 200 nm from the line core (Burrows et al. 2000). Figure 3 shows the i' and z' filters superimposed on two different model spectra. The i' filter is centered on the K I doublet core and the z' filter probes the far red wing. The brown dwarf colors become redder in $i' - z'$ for decreasing T_{eff} because these filters probe the Wein tail of the Planck function and the K I doublet gets stronger. The gradual disappearance of TiO and cloud opacity as T_{eff} decreases leaves behind a nearly transparent atmosphere at wavelengths below 1 μm (Figure 2) and reveals the K I doublet in all its pressure-broadened splendor. At low T_{eff} ($\sim 700\text{ K}$) the $i' - z'$ redward trend halts as K I is depleted into KCl and the doublet weakens.

Given the dependence of the $i' - z'$ color on the K I resonance doublet, this color provides a stringent test for chemical equilibrium models. The two sets of curves in Figure 1b show colors computed with and without condensate sedimentation in the chemical equilibrium. There is a substantial difference — of 2 magnitudes — in $i' - z'$ at effective temperatures where the K I line is prominent ($\sim 800\text{ K}$). The major difference between the two approaches is that at temperatures below 1400 K, the monatomic K abundance (hence the opacity) is much lower under the assumption of no sedimentation (BS99) than under the assumption of sedimentation (Lodders 1999). A comparison of spectra computed under both assumptions is shown in Figure 3. The effect on the $i' - z'$ color is rather dramatic and the models without sedimentation turn blueward well before the model that includes sedimentation, as shown in Figure 1.

The two different assumptions used to model chemical equilibrium of gas and condensates give such different results that they are worth discussing in more detail. The two models depend on the physical setting (see Lodders 1999; Lodders & Fegley 2001). In the no-sedimentation case condensates remain in local equilibrium with the gas. In cooler regions, the high temperature (primary) condensates react with the upper atmospheric gas to form secondary condensates via gas-solid reactions. Complete chemical equilibrium exists between all phases in this no-sedimentation case. BS99 term this case the “no rainout” approach. Their approach (also employed by e.g. Chabrier et al. 2000; Allard et al. 2001) implies that alkali elements such as Na and K condense into alkali feldspar ($(\text{Na},\text{K})\text{AlSi}_3\text{O}_8$) after a long sequence of primary condensate reactions with the gas. The net effect in this no-sedimentation case is that the gaseous atomic K and Na become depleted in the atmosphere once alkali feldspar condenses.

As pointed out by Lodders (1999) and Lodders & Fegley (2001), however, this approach does not apply to brown dwarf and giant planet atmospheres because a gravity field is acting on condensates. The primary condensates are sequestered by sedimentation into a cloud and are not available for gas-solid reactions in the atmosphere above the cloud layer as the brown dwarf cools. These cloud condensation models have been used successfully for over 30 years in the planetary community (Lewis 1969, Barshay & Lewis 1978, Fegley & Lodders 1994) and were recently termed “rainout”

by BS99. We prefer to avoid this term⁸. In the sedimentation case, elements such as Al and Ca condense out at greater depth and are consequently absent in the overlying atmosphere. Thus alkali feldspar cannot form and Na and K remain in the gas phase. Only when the brown dwarf is much older and cooler ($T_{\text{eff}} \sim 700 \text{ K}$) are atmospheric temperatures low enough for monatomic Na and K to convert into chloride and hydroxide gasses and eventually condense, at even cooler temperatures, as Na_2S and KCl .

The $i' - z'$ color is sensitive to pressure broadening of the K I doublet. The exceptionally strong pressure broadening affecting the $0.59 \mu\text{m}$ Na I and the $0.77 \mu\text{m}$ K I resonance doublets in T dwarfs stretches the current theories of line broadening beyond their limit of validity. These lines are modeled with a far wing exponential cutoff $\exp -(qh\Delta\nu/kT)$ where q is an undetermined parameter of order unity⁹. A detailed discussion is given in Burrows et al. (2000) as well as fits of the optical spectra of Gl 229B and SDSS 1624+00. With abundances determined from the sedimentation chemistry of Lodders (1999), we have obtained good fits of the optical spectra of Gl 229B and Gl 570D with $q = 1$ (Geballe et al. 2001). The $i' - z'$ color changes by as much as 0.4 mag for models computed with $q = 0.5$ and $q = 1$. Disentangling the line broadening parameters from other $i' - z'$ color effects will likely come from fitting high resolution spectra.

4.3. The Coolest Brown Dwarfs

The coolest brown dwarf known with a reliable determination of its effective temperature is Gl 570D with $T_{\text{eff}} \sim 800 \text{ K}$ (Geballe et al. 2001). Cooler brown dwarfs are expected to enter a new regime in the $i' - z'$ vs. $J - K$ color space than those discovered so far. Brown dwarfs with $T_{\text{eff}} \lesssim 600 \text{ K}$ have water clouds forming in the upper atmosphere. Just as the subsidence of silicate clouds below the photosphere causes a turnover in colors, the appearance of water clouds in the upper reaches of low- T_{eff} atmospheres could have severe effects on the colors.

At relatively cool T_{eff} ($\sim 600 \text{ K}$), as K I disappears into KCl , the $i' - z'$ color reaches a maximum and turns over blueward as shown by the coolest objects in Figure 1. The formation of significant ($\tau > 0.1$) water clouds below $T_{\text{eff}} \sim 500 \text{ K}$ (depending on g) halts and may eventually reverse the blueward march in $J - K$ with decreasing T_{eff} because the water cloud acts like a blackbody, redistributing the flux to the blackbody peak. In fact the models presented here may underestimate the size of the redward turn in $J - K$. Smaller particles than the ~ 20 to $30 \mu\text{m}$ predicted by the cloud model would arise for smaller values of the unconstrained stratospheric eddy diffusion constant and would produce more cloud opacity for $T_{\text{eff}} \leq 500 \text{ K}$. Such objects will be very faint at z' and will be difficult to detect with SDSS. Nevertheless, the number density of brown dwarfs suggests that there may be one nearby which could be detected by SIRTF (Martin et al.

⁸It is ambiguous whether the term applies to condensate falling within a cloud or from the base of a cloud.

⁹ q may be measured experimentally in the near future (A. Dalgarno, private communication).

2001).

5. Discussion

The $i' - z'$ vs. $J - K$ color-color diagram reveals the importance of sinking, precipitating condensation clouds in controlling the colors of the L dwarfs and of the transition between L and T dwarfs, and will complement high resolution spectroscopy (Griffith & Yelle 2000; Geballe et al. 2001) to reveal the nature of condensation chemistry in these atmospheres.

Most previous and current brown dwarf models (e.g. Allard et al. 1996; Marley et al. 1996; Tsuji et al. 1996; Burrows et al. 1997; Chabrier et al. 2000; Allard et al. 2001) considered either the case in which condensates remain suspended in the atmosphere or considered them to be absent from the photosphere due to sedimentation (although Tsuji 2001 presents an heuristic condensate model). Both Allard et al. (2001) and Tsuji (2001) assume a fixed, submicron, particle size distribution derived from interstellar medium dust grains. Allard et al. correctly point out that as long as the particle size is smaller than the wavelength of light, Rayleigh scattering dominates the opacities and the exact size distribution of particles has little effect on the opacities. They also argue that particle sizes larger than $100 \mu\text{m}$ are implausible because they would break up (terrestrial raindrops and billiard-ball sized hailstones bely this assertion). The cloud model of Ackerman & Marley (2001) used here predicts silicate and iron particle sizes between $10\text{--}100 \mu\text{m}$. Thus the predicted particle size is greater than the wavelength of observation and the size distribution cannot be ignored.

Interpreting the objects intermediate between the cloudy L dwarfs and the cloudless coolest T dwarfs—i.e. the blueward turn in $J - K$ in Figure 1 — requires an understanding cloud formation in brown dwarf atmospheres. The models used here are the first to employ a self-consistent vertical cloud model in which particle sizes and distribution are computed from cloud physics (Ackerman & Marley 2001). Depending on the parameter of the chosen cloud model (f_{rain} , see Fig.1a), a very different color path can result. Nevertheless, the best fitting f_{rain} parameter probably varies with T_{eff} , and a more detailed model may be needed.

We have shown the benefits of optical and IR colors for potentially understanding clouds and alkali metal chemistry. High resolution spectroscopy may not be possible or necessary for all of the few hundred brown dwarfs expected from SDSS and 2MASS. The discovery of more brown dwarfs in this “cloud transition” regime (late L to early T) is expected in the near future from the SDSS. Brown dwarf $i' - z'$ colors will reveal which treatment of the equilibrium chemistry in brown dwarf atmospheres is correct. Since the best-fitting cloud model predicts that cloud particles are not lofted much above the cloud base, the sedimentation chemistry is likely most appropriate, in agreement with expectations. A complete test of this hypothesis, however, requires follow up observations since brown dwarfs are usually not detected in i' band by the SDSS survey. The follow up photometry is in progress.

We thank Adam Burrows for use of the results from his chemical equilibrium model and alkali gas opacity table. M.M. acknowledges support from NASA grants NAG2-6007 and NAG5-8919 and NSF grants AST-9624878 and AST-0086288. S.S. is supported by the W.M. Keck Foundation, and work by K.L. and D.S. is supported by NSF grant AST-0086487 and NASA grant NAG54988, respectively.

REFERENCES

Ackerman, A. & Marley, M. 2001 *ApJ*, in press, arXiv:astro-ph/0103423

Allard, F., Hauschildt, P. H., Baraffe, I., & Chabrier, G. 1996, *ApJ*, 465, L123

Allard, F. et al. 2001, *MNRAS*, in press, arXiv:astro-ph/0104256

Barshay, S. S. & Lewis, J. S. 1978, *Icarus*, 33, 593

Burgasser, A. J. et al. 1999, *ApJ*, 522, L65

Burgasser, A. J. et al. 2000, *AJ*, 120, 1100

Burrows, A. et al. 1997, *ApJ*, 491, 856

Burrows, A., Marley, M. S., & Sharp, C. M. 2000, *ApJ*, 531, 438

Burrows, A., & Sharp, C. M. 1999, *ApJ*, 512, 843 (BS99)

Chabrier, G., Baraffe, I., Allard, F., & Hauschildt, P. 2000, *ApJ*, 542, 464

Chamberlain, J. W. & Hunten, D. M. 1987, Orlando FL Academic Press Inc International Geophysics Series, 36

Fan, X. et al. (SDSS) 2000, *AJ*, 119, 928

Fegley, B. J. & Lodders, K. 1994, *Icarus*, 110, 117

Fegley, B. J. & Lodders, K. 1996, *ApJ*, 472, L37

Fukugita, M., Ichikawa, T., Gunn, J. E., Doi, M., Shimasaku, K., & Schneider, D. P. 1996, *AJ*, 111, 1748

Geballe, T. et al. *ApJ*, in press, arXiv:astro-ph/0103187

Griffith, C. & Yelle, R. 2000, *ApJ*, 532, L59

Kirkpatrick, J. D. et al. 1999, *ApJ*, 519, 802

Kirkpatrick, J. D., Reid, I. N., Liebert, J., Gizis, J. E., Burgasser, A. J., Monet, D. G., Dahn, C. C., Nelson, B., & Williams, R. J. 2000, *ApJ* 120, 447

Leggett, S. K., Allard, F., & Hauschildt, P. H. 1998, *ApJ*, 509, 836

Leggett, S. K. et al. (SDSS) 2000, *ApJ*, 536, L35

Lewis, J. S. 1969, *Icarus*, 10, 365

Lodders, K. 1999, *ApJ*, 519, 793

Lodders, K. & Fegley, B. 2001, submitted to ApJ

Marley, M. 2000, From Giant Planets to Cool Stars, ASP Conference Series, Vol. 212. Edited by C.A. Griffith and M.S. Marley. (San Francisco: ASP), p.152

Marley, M. S., Saumon, D., Guillot, T., Freedman, R. S., Hubbard, W. B., Burrows, A., & Lunine, J. I. 1996, Science, 272, 1919

Martin, E. L., Delfosse, X., Basri, G., Goldman, B., Forveille, T., & Zapatero Osorio, M. R. 1999, AJ, 118, 2466

Martin, E. L., Brandner, W., Jewitt, D. C., Simon, T., Wainscoat, R., Connelley, M., Marley, M., & Gelino, C. 2001, PASP, 113, 529

Reid, N. et al. ApJ, in press

Saumon, D., Geballe, T. R., Leggett, S. K., Marley, M. S., Freedman, R. S., Lodders, K., Fegley, B., & Sengupta, S. K. 2000, ApJ, 541, 374

Strauss, M. et al. (SDSS) 1999, ApJ, 522, L61

Tsuji, T., Ohnaka, K., Aoki, W., & Nakajima, T. 1996, A&A, 308, L29

Tsuji, T., Ohnaka, K., & Aoki, W. 1999, ApJ, 520, L119

Tsuji, T. 2001, in press, arXiv:astro-ph/0103395

Tsvetanov, Z. I. et al. (SDSS) 2000, L61

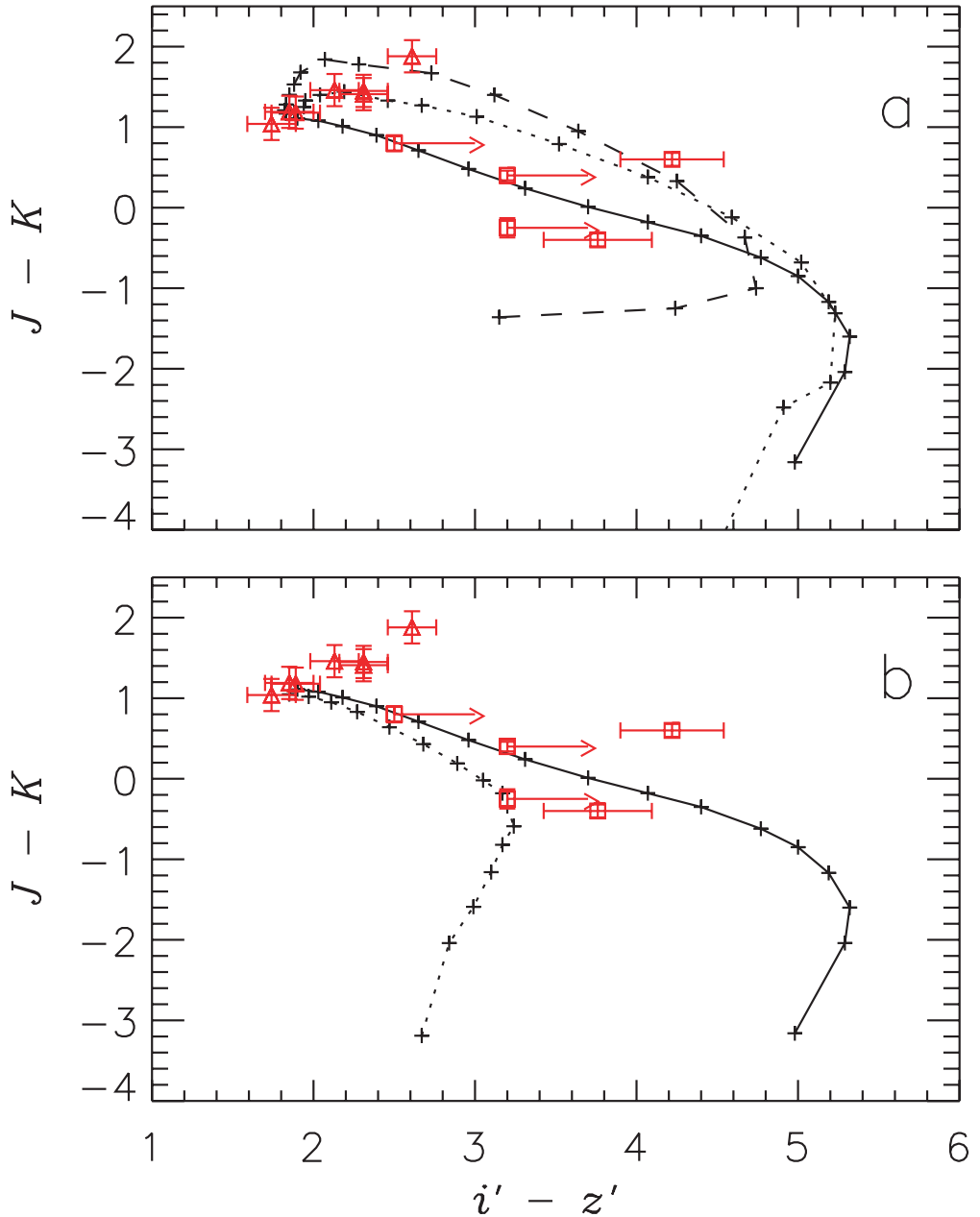


Fig. 1.— $i' - z'$ (SDSS) vs. $J - K$ (UKIRT) color-color diagram for brown dwarfs. The triangles and squares are observed L dwarfs and T dwarfs respectively (Strauss et al. 1999; Fan et al. 2000; Legett et al. 2000; Tsvetanov et al. 2000). The lines show our theoretical models with the symbols representing T_{eff} steps of 100 K in the T_{eff} range 2000 K – 400 K. Panel (a) shows the difference between cloudy models (dotted and dashed lines) and cloudless models (solid line) for $g = 1000 \text{ m s}^{-2}$. The dashed and dotted lines show cloudy models computed with $f_{\text{rain}} = 3$ and $f_{\text{rain}} = 5$, respectively. Panel (b) shows cloudless brown dwarf models with $g = 1000 \text{ m s}^{-2}$. The solid line shows brown dwarf models with the sedimentation chemical equilibrium model by Lodders and the dotted line are models using the BS99 chemical equilibrium model with no condensate sedimentation. See §3 and §4 for details.

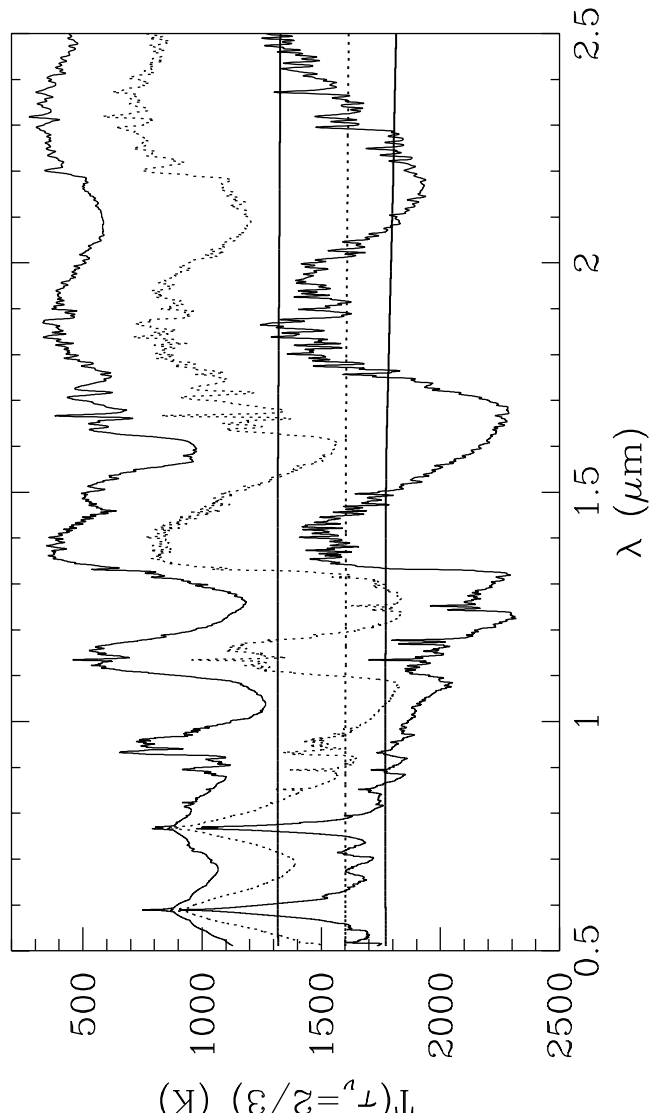


Fig. 2.— Visibility of the cloud layer in brown dwarfs as a function of T_{eff} . The curves show the depth of the photosphere ($\tau_{\nu} = 2/3$), indicated by the temperature in the atmosphere, as a function of wavelength. The y-axis is essentially a brightness temperature. Three models with $g = 1000 \text{ m s}^{-2}$ and $f_{\text{rain}} = 5$ are shown, from top to bottom $T_{\text{eff}} = 500, 1000$ (dotted), and 1500 K , respectively. Two curves are shown for each model, one showing the photosphere due to gas opacity only, and one due to cloud opacity only. The latter is very flat, due to the nearly grey cloud opacity, and shows the level where the cloud becomes optically thick. At wavelengths longer than shown

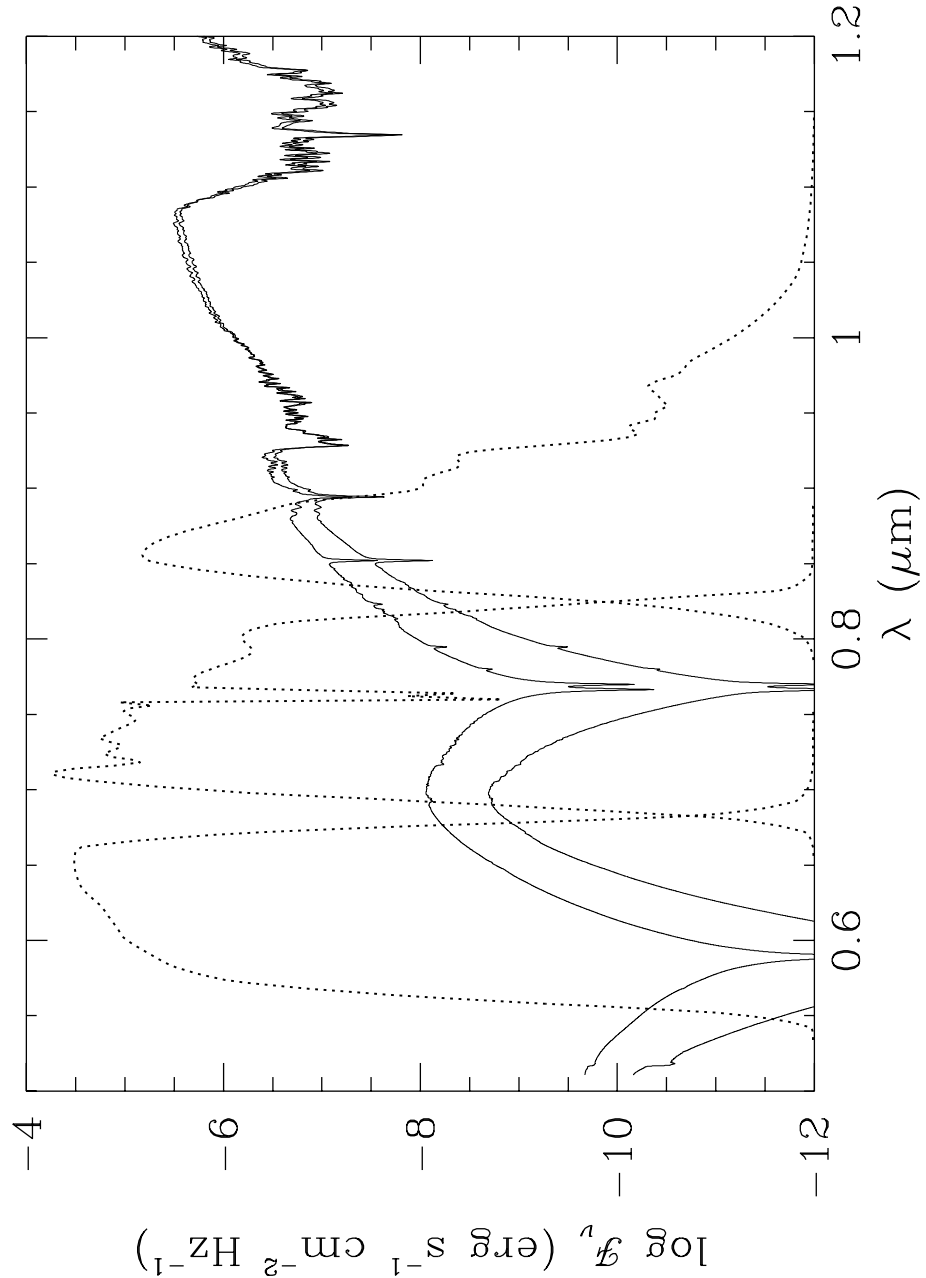


Fig. 3.— SDSS r' , i' , and z' transmission curves (dotted lines from left to right, respectively) superimposed on brown dwarf model spectra. The i' flux is controlled by the K I doublet line core and the z' flux by the K I doublet wing. These cloudless synthetic spectra with $T_{\text{eff}} = 1000$ K and $g = 1000 \text{ m s}^{-2}$ are computed with the chemical abundances of BS99 (i.e. no sedimentation assumed; upper curve) and of Lodders (with condensate sedimentation; lower curve). The effect of the chemical equilibrium model on the strength of the K I and Na I doublets is very noticeable. See §3 and §4.2 for details.